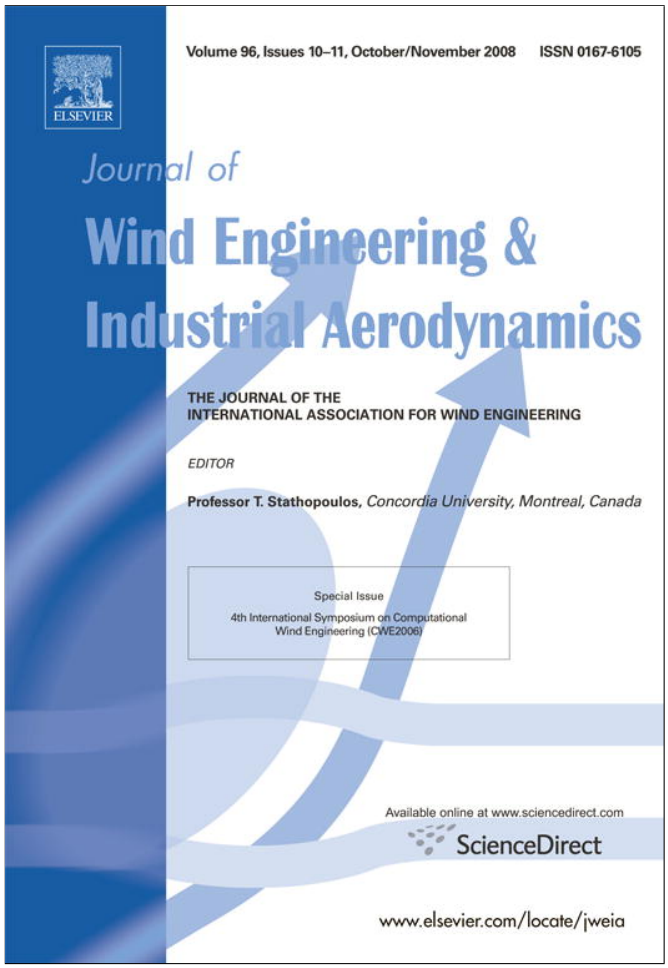

ELSEVIER

Journal of Wind Engineering
and Industrial Aerodynamics 96 (2008) 1789–1804

JOURNAL OF wind engineering AND industrial aerodynamics

www.elsevier.com/locate/jweia

Protocol for CFD prediction of cooling-tower drift in an urban environment

Robert N. Meroney

Civil and Environmental Engineering Department, Colorado State University, Fort Collins, CO, USA

Available online 18 April 2008

Abstract

A computational fluid dynamics (CFD) code including Lagrangian prediction of the gravity driven but stochastic trajectory descent of droplets is considered to predict plume rise and surface drift deposition from mechanical draft cooling towers. CFD drift deposition calculations are performed for a specific urban cooling-tower situation with and without the urban buildings surrounding the cooling-tower complex present to produce a set of multiplicative factors that could be used to correct seasonal or annual predictions for the presence of large urban structures.

Keywords: Drift; Deposition; Cooling tower; Urban pollution

1. Introduction

Drift of small water droplets from mechanical and natural draft cooling-tower installations can contain water treatment chemicals such that contact with plants, building surfaces and human activity can be hazardous. Prediction of drift deposition is generally provided by analytic models such as the US Environmental Protection Agency approved ISCST3 (Industrial Source Complex Short Term Version 3) (US EPA, 1995) or SACTI (Seasonal-Annual Cooling Tower Impact) (Policastro et al., 1981) codes; however, these codes are less suitable when cooling towers are located midst taller structures and buildings. A computational fluid dynamics (CFD) code including Lagrangian prediction of the gravity driven but stochastic trajectory descent of droplets was previously considered and compared to data from the 1977 Chalk Point Dye Tracer Experiment

E-mail address: Robert.Meroney@colostate.edu

0167-6105/$ - see front matter
doi:10.1016/j.jweia.2008.02.029

(Meroney, 2006). The CFD program predicted plume rise, surface concentrations, plume centerline concentrations and surface drift deposition for the Chalk Point study within the bounds of field experimental accuracy. Similar CFD Lagrangian discrete phase model (DPM) techniques have been used successfully to predict rain fall deposition in valleys and on buildings (Blocken and Carmeliet, 2006; Blocken et al., 2006). This paper recommends a CFD protocol to correct drift and deposition predictions provided by familiar analytic models for building effects.

1.1. Prediction of cooling-tower plume behavior

Meroney (2006) reviewed experimental and numerical research related to the flow around and from natural and mechanical draft cooling towers. A number of previous researchers have used CFD to calculate cooling-tower plume rise, dispersion, moisture visibility, and building interaction. England et al. (1973) used a three-dimensional CFD code to calculate dry and wet cooling-tower plume behavior downwind of the Keystone Power Plant in western Pennsylvania. Bergstrom et al. (1993) reported the results of a two-dimensional simulation of the interaction of the flow through an idealized cooling tower with the wind flow over the tower. Later Derksen et al. (1996) and Bender et al. (1996a, b) reported on a wind tunnel and numerical study on the effects of wind on air intakes and flow rates of a cooling tower. Takata et al. (1996) calculated the effects of wind on the visible envelope of moist cooling-tower plumes. No CFD calculations were found in the literature that predicted drift deposition levels downwind of cooling towers. Hence, Meroney (2006) examined the use of a Lagrangian discrete particle method to predict drift measured during the 1977 Chalk Point Dye Tracer Experiment. His results confirmed that such an approach could predict plume rise, ground concentrations, and deposition magnitudes for an isolated cooling-tower situation.

The movement of cooling-tower drift can be calculated via various multi-phase mixing models. Eulerian–Lagrangian models calculate the background flow field using conventional RANS or LES solution procedures, and then individual particles are tracked in space using discrete phase models (DPM). Eulerian–Eulerian models treat the droplets as a separate dispersed phase and both the background flow field and the droplet species are calculated using Reynolds averaged Navier Stokes (RANS) or large eddy simulation (LES) turbulence models. Sometimes both methods can be used to provide a crosscheck on computational reliability (Fluent 6.1 User's Guide, 2003). The DPM methodology has been used for this study.

1.2. Creation of a CFD protocol to correct drift for building effects

In order to evaluate the long-term health effects of droplet drift and deposition accumulation from a source such as a cooling tower, it is appropriate to accumulate information for seasonal and annual periods that include the actual distribution of wind orientations, wind speeds, and humidity and thermal conditions observed at the location. Unfortunately, most CFD methods which include building configurations and adjust for enhanced turbulence and downwash in the building wakes are not conveniently applied to the superposition of such a wide range of situations due to computational time and economic constraints. On the other hand, computationally efficient analytic codes such as SACTI (Policastro et al., 1981) which do permit seasonal and annual weighting of

air pollution drift and deposition predictions do not incorporate the full effects of building wakes.

Hence, a method was sought to adjust or calibrate analytic drift code predictions for building effects using CFD results. This paper considers CFD calculations performed for a specific urban cooling-tower situation with and without the urban buildings surrounding the cooling-tower complex present to produce a set of multiplicative factors that could be used to correct conventional seasonal or annual drift model predictions for the presence of large urban structures.

Similar amplification factors have been proposed before to account for terrain effects on gaseous dispersion using experimental measurements in wind tunnel and water channels (Lawson et al., 1989; Snyder, 1990). This idea has also been extended to numerical prediction of amplification factors of terrain effects on gaseous dispersion (Brucher, 2001). Finally, corrective factors based on wind-tunnel measurements have even been used in European Union regulatory situations to adjust ground-level concentrations produced by discharges from cooling towers for building effects (Bahmann and Schmonsees, 2004). In the latter case measurements resulted in relative increases in predicted annual concentrations downwind of cooling towers ranging from 1.1 to 7.7 over distances out to 4 km. The authors noted that at present the method has only been used in impact statements based on discussions reached between consultants and responsible local authorities, and it has not yet been incorporated into government standards.

1.3. Urban complex test case

It is anticipated that the presence of tall upwind buildings, terrain elevation changes and irregular arrangement of buildings in an urban area will accelerate droplet deposition downwind of a cooling-tower facility. Downdrafts and turbulence associated with building wakes are known to accelerate the downward motion of drift particles. Several computational domains were created to study a set of actual mechanical draft cooling towers located surrounded by a downtown section of a major US city. The domain dimensions were typically 600 m long, 300 m wide and 150–230 m deep with a mixture of from 1.5 to 2.5 million hexagonal and tetrahedral cells. Building heights within the domain ranged from 3 to 175 m tall with footprints ranging from 6 to 23,000 sq m (see Fig. 2). Domain was chosen to reflect the model extent of a parallel wind-tunnel model study; hence, it did not necessarily meet the boundary stand-off recommendations of recent validation studies. Nonetheless, comparisons of wind-tunnel flow visualization videos with particle track motions during the numerical study suggested effects were minimal.

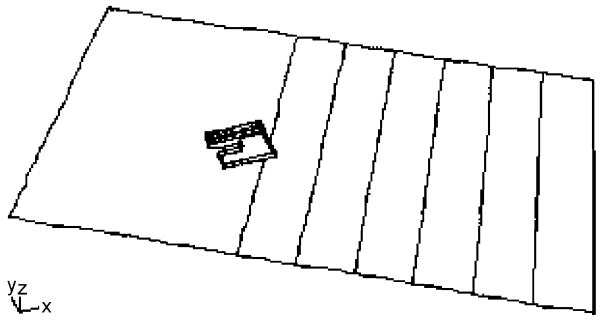

Fig. 1. Isolated CT including 75 m wide zones, 180°.

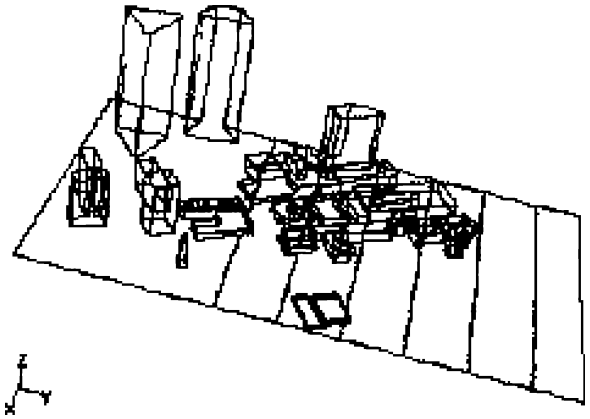

Fig. 2. CT in urban area with 75 m wide zones, 180°.

The cooling-tower facility consisted of 11 units in a U-shaped tower/turbine building complex which emitted plumes from stacks 12 m above grade (see Figs. 1 and 2).

2. Computational fluid modeling

The commercial software selected for these calculations solves the three-dimensional Reynolds averaged equations of motion discretized using a control volume approach for flow, pressure, turbulence, and concentration distributions (Fluent 6.1 User's Guide, 2003). The Reynolds stress terms are modeled by one of several turbulence models. Since in this study the behavior of cooling-tower drift is emphasized and not detailed flow or surface pressures in bluff-body separation and recirculation zones, the standard κ–ε turbulence model with standard wall functions was considered adequate. Recent CFD calculations of flow in urban areas have satisfactorily used the standard $k-\varepsilon$ model (Yoshie et al., 2006; Zhang et al., 2005) producing wind speeds within 10% of experimental measurements. The standard $k-\varepsilon$ turbulence model assumes isotropic turbulence and uses transport equations for the turbulent kinetic energy (k) and its dissipation rate (ε). Ground and wall surfaces were specified as rigid planes with zero roughness. Inlet (upwind) velocity and turbulence profiles were selected to reproduce field observations. Lateral and upper boundaries were specified as symmetry boundaries with slip velocity conditions.

2.1. Discrete phase modeling

Once a total flow field is defined, the software may be configured to calculate the Lagrangian particle tracks of drift droplets emitted from the cooling-tower exhaust nozzles. Particle sizes can be uniform or a specified particle distribution. Particle material can be inert or droplets that undergo evaporation and change in diameter over their lifetime. Particle trajectories can be calculated as simple ballistic trajectories uninfluenced by turbulence, or they can include stochastic dispersion due to the weighted effects of local turbulence and wind speed variations. For the Lagrangian stochastic approach droplets are released from the cooling-tower stack and their movement tracked based on the pre-calculated mean wind field and turbulence properties predicted by the RANS model. The particle positions are obtained by integrating the trajectory equations using the

instantaneous fluid velocities ($U_i + u_i'$) along the particle path, where U_i are the mean velocity components and u_i' are the velocity fluctuations related to the local turbulence intensity through a normally distributed random number, which is constant for each "eddy lifetime". It is assumed here that the turbulent intensity distributions predicted by the k–ε tubulence model adequately predict particle dispersion; however, this has not been verified. Particles which intersect a wall are presumed to deposit, not bounce or re-entrain.

If deposition predictions are to be made, an informed selection of a "reasonable" droplet distribution is necessary. A review of the literature by Meroney (2006) produced nine sets of data for the cumulative mass fraction distributions of droplets. The cumulative mass fraction for these cases tended to decrease exponentially with increasing particle diameter; hence, the data were fit to a Rosin–Rammler particle distribution of the form:

$$\text{Cum Mass Fraction} = \exp(-(d/d_{\text{mean}})^n),$$

where d_{mean} is the mean particle diameter, and n is known as the shape factor. Data seem to fall into two categories with either $d_{\text{mean}} \sim 0.1$ mm and $n = 1.0$ or $d_{\text{mean}} \sim 1.0$ mm and $n = 1.0$. The second category reflects the presence of a significant number of large particles. Droplet distributions often have more large droplets than manufacturers like to admit due to end losses, splash and condensation on the cooling-tower structure with subsequent re-entrainment, or due to poor maintenance and structure deterioration. For the purpose of this example situation conditions with $d_{\text{mean}} = 0.1$ mm and $n = 1.0$ were used.

Alternatively, the software can be configured to simultaneously calculate fluid motions and particle behavior. This option permits the inclusion of phase change effects on plume rise and droplet size as the particles evaporate or condense during travel; however, inclusion of this option can significantly increase computational time since the calculation requires a full transient solution. Since large particles were the primary emphasis of this analysis for which time of flight were short, evaporation was not considered.

2.2. Drift from isolated cooling-tower complex

The proposed multiple cooling-tower unit, U-shaped cooling tower/boiler complex was modeled as an isolated facility within a domain approximately 600 m long, 300 m wide and 150 m deep with about 1.5 million hexagonal and tetrahedral cells. Approach wind and turbulence profiles were set to simulate winds flowing over suburban sections of a city with three wind speeds (2.5, 5.0 and 7.5 m/s at a height of 52 m, power law coefficient equal to 0.25), and droplets were emitted vertically in an air/vapor plume at 8.5 m/s from the cooling-tower units 1 through 11 at a rate of 1 kg/s/unit and a specified droplet distribution. Note that 1-μm droplets are transported out the end of the domain without ground deposition (Fig. 3), whereas 500-μm particles begin to accumulate immediately (Fig. 4). Particles released in a complete Rosin–Rammler distribution ($d_{\text{mean}} = 0.1$ mm, $n = 1$) produce deposition of large particles out to 450 m with smaller particles transporting out of the domain (Fig. 5). Fig. 6 displays the contours of ground-level droplet deposition magnitude. Since there are no upwind obstructions to produce wind veering or wake turbulence, the particles fall in a narrow path about 40 m wide extending directly downwind from the cooling-tower building. Figs. 3–6 are for wind approach angles of 160°, but results are similar for other wind orientations.

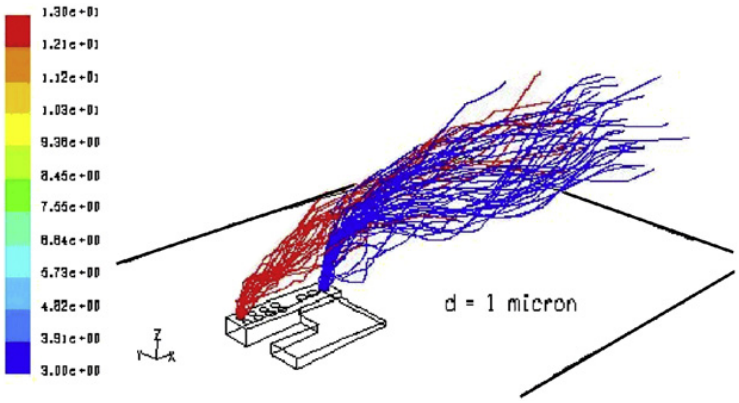

Fig. 3. DPM predicted particle tracks from Units 1 and 11 for 1 μm diameter particles. 160° wind angle.

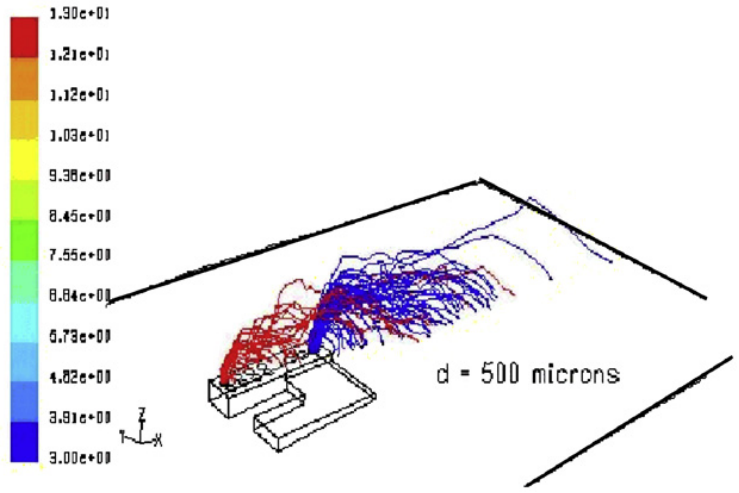

Fig. 4. DPM predicted particle tracks from Units 1 and 11 for 500 μm diameter particles. 160° wind angle.

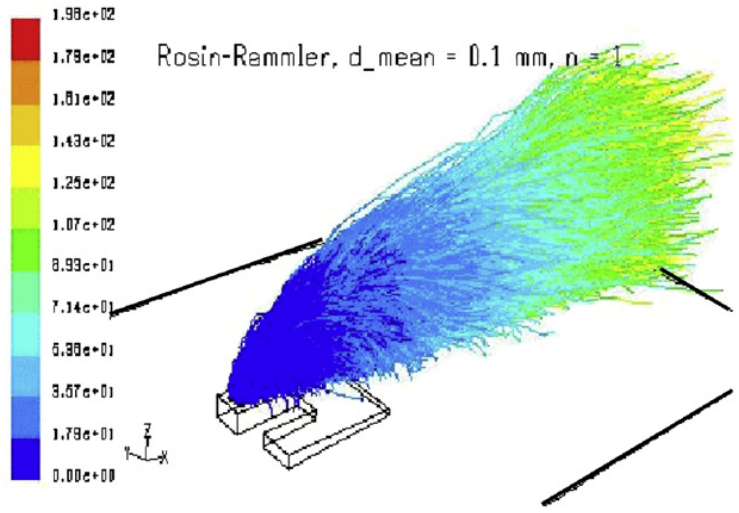

Fig. 5. DPM particle tracks from Units 1 to 11 for Rosin–Rammler distribution ($d_{mean} = 0.1$ mm, $n = 1$). 160° angle.

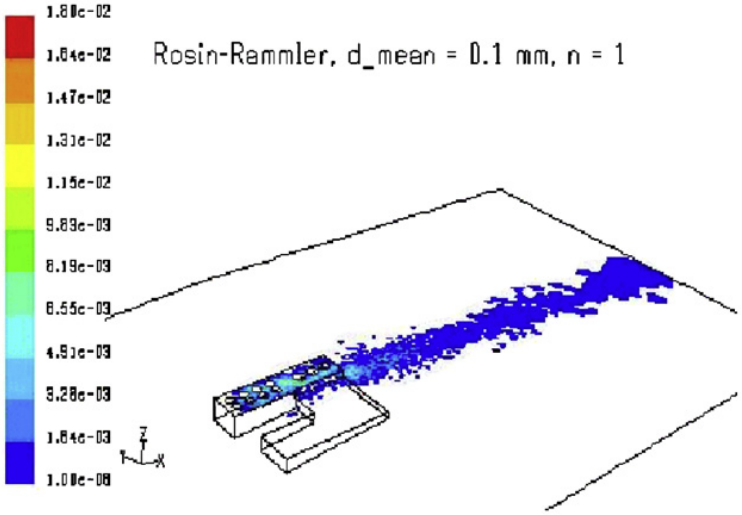

Fig. 6. DPM predicted nodal contours of deposition for Units 1–11 (kg/m^2 s). 160° wind angle.

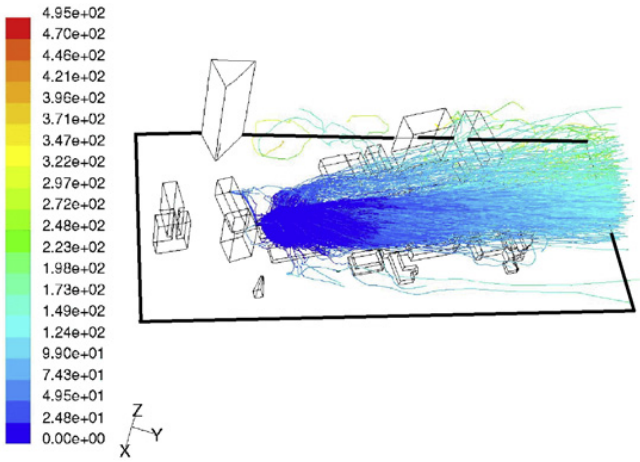

Fig. 7. DPM predicted particle tracks from Units 1 to 11 for wind approach angle 160° and Rosin–Rammler source distribution ($d_{mean} = 0.1$ mm, $n = 1$).

2.3. *Drift from a cooling-tower complex within an urban environment*

It is now appropriate to consider how the cooling-tower plumes behave in the presence of large upwind and downwind structures. Calculations were completed for wind approach angles of 160°, 180°, 220° and 240° from north, the same approach wind conditions stipulated during the isolated cooling-tower calculations, and all cooling-tower units operating under full load conditions. Flow and particle source conditions were the same as discussed in Section 2.1.

Results for wind direction 160° : Fig. 7 displays the droplet particle tracks produced by a release of particles representative of a Rosin–Rammler droplet distribution with $d_{mean} = 0.1$ mm and shape factor, $n = 1$. Particles are trapped on the grounds and buildings of the entire building complex directly downwind and even recirculate into the wake region of the tall structure to the west of the cooling-tower source. Fig. 8 plots the contours of nodal values of the droplet deposition rates (these values are actually about 30–50% less than face values due to interpolation). Note that deposition is spread laterally

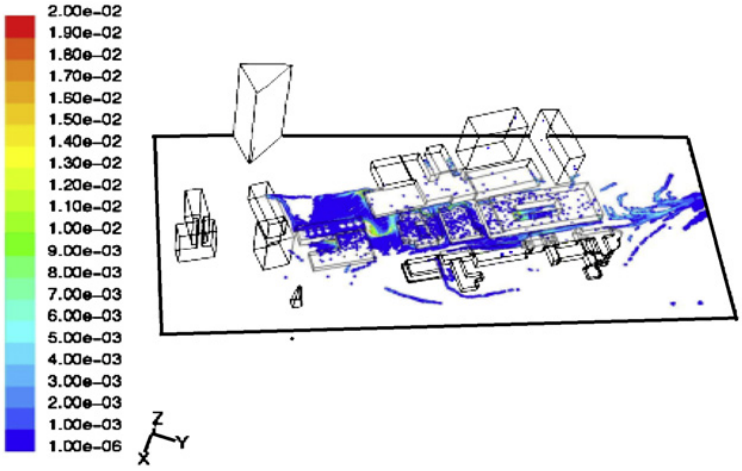

Fig. 8. DPM predicted nodal contours of deposition for Units 1–11 (kg/m^2 s) for wind approach angle 160°.

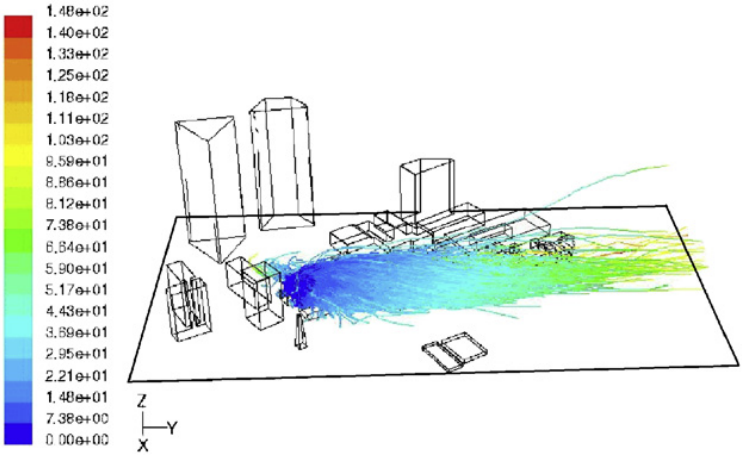

Fig. 9. DPM predicted particle tracks from Units 1 to 11 for wind approach angle 180° and Rosin–Rammler source distribution ($d_{mean} = 0.1$ mm, $n = 1$).

by local wind flow and turbulent gusts. For the same initial conditions the building turbulence and wind deflections bring more of the small particles to the ground faster; hence accretion rates are still as large as the maximum isolated deposition values 350 m downwind! The presence of buildings increases the drift deposition by a factor of 10 over an isolated release for distances from 150 to 300 m downwind.

Results for wind direction 180° : For a shift in wind direction of only 20° significant differences in dispersion and deposition occur (Fig. 9). Wind approaches the cooling-tower complex from upwind passing between the four primary upwind structures. Particle tracks do not ascend as high in the large updrafts found for 160°. Deposition contours (Fig. 10) suggest most of the large depletion occurs in the first 150 m downwind, perhaps because the finer particles are now escaping the region and are not caught within the recirculation zones in the open spaces and courtyards downwind.

Results for wind direction 220° : Figs. 11 and 12 may now be compared with the two earlier figure sets 7–8 and 9–10, respectively. Most of the transport and dispersion occurs to the northeast impacting only open spaces, but there is evidence of a strong clockwise swirl upwards. This rotation may be attributed to the wakes of the large 175 m tall towers to the west. Fig. 12 suggests that deposition rates are still large near the cooling tower and

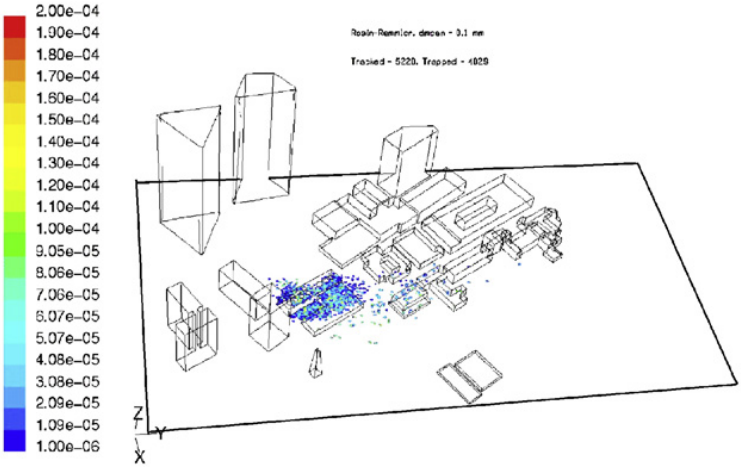

Fig. 10. DPM predicted nodal contours of deposition for Units 1–11 (kg/m^2 s) for wind approach angle 180°.

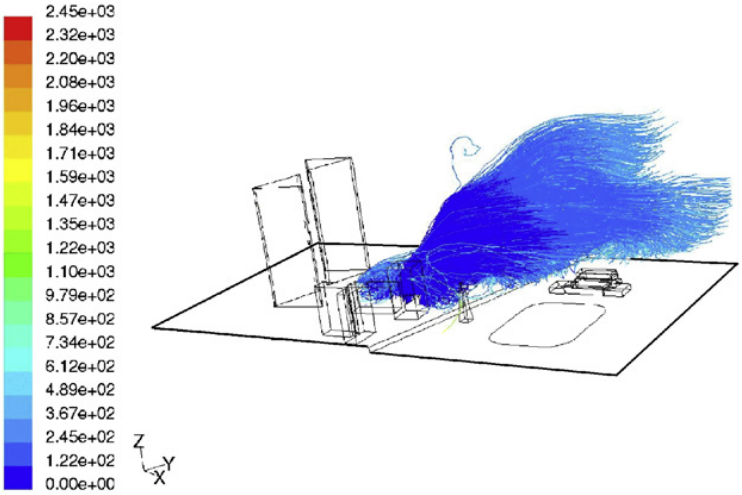

Fig. 11. DPM predicted particle tracks from Units 1 to 11 for wind approach angle 220° and Rosin–Rammler source distribution ($d_{mean} = 0.1$ mm, $n = 1$).

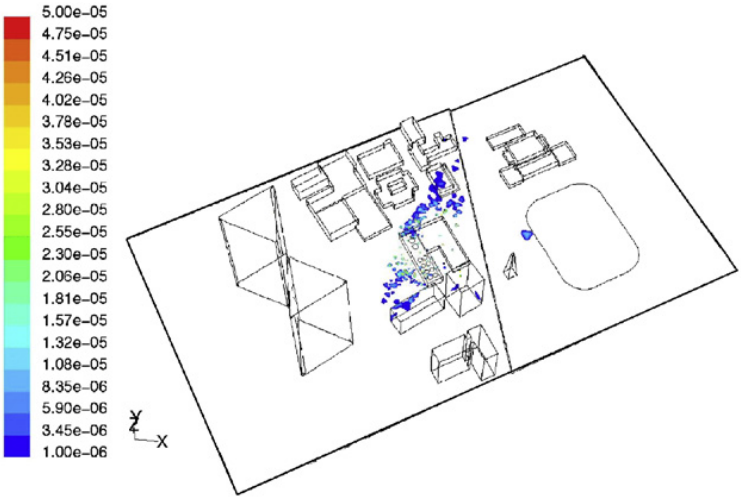

Fig. 12. DPM predicted nodal contours of deposition for Units 1–11 (kg/m^2 s) for wind approach angle 220°.

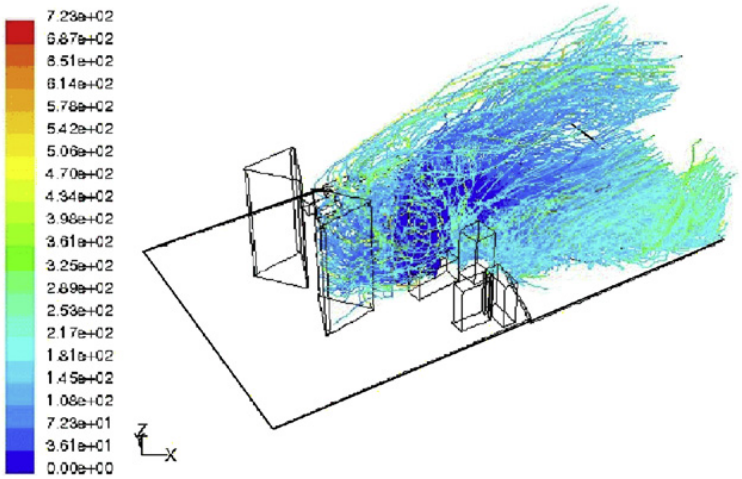

Fig. 13. DPM predicted particle tracks from Units 1 to 11 for wind approach angle 240° and Rosin–Rammler source distribution ($d_{mean} = 0.1$ mm, $n = 1$).

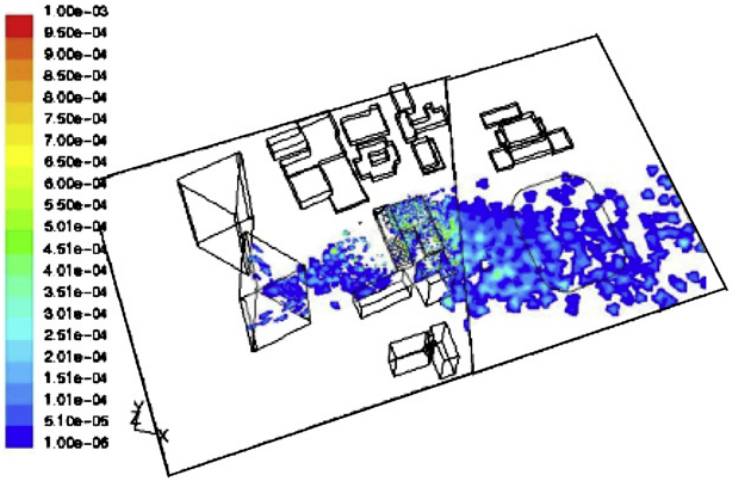

Fig. 14. DPM predicted nodal contours of deposition for Units 1–11 (kg/m^2 s) for wind approach angle 240°.

a large number of droplets impact the ground upwind and on top of the cooling-tower facility.

Results for wind direction 240° : Compare Figs. 13 and 14 with the three earlier figure sets 7–8, 9–10 and 11–12, respectively. Approach winds now pass directly over and between the two 150 m tall upwind skyscrapers. Water vapor from the cooling towers is entrained directly into the wakes of the skyscrapers, but winds passing between the two towers deflect the cooling-tower plumes to the south and east. Fig. 14 shows a particle track picture that looks like a mass of snarled yarn. Small particles are lofted upwind and upward, after which they flag downwind of the skyscraper and escape the computation domain. But other particles are carried to the east passing over the open regions and depositing heavily on ground surfaces.

3. Zonal calculation of deposition rates

The program also has an option to track total mass accumulation rates on designated surfaces (or zones) as well as perform total mass balances on the particles released from the

source locations. Thus, it was decided to divide the downwind ground and building regions into discrete swaths or zones 76 m wide perpendicular to each wind orientation extending from the downwind edge of the cooling-tower facility out to about 381 m. This distance extends beyond the limits of the primary deposition region. In real flows local gustiness will divert the instantaneous approach wind direction, but zonal deposition integrated over lateral segments should be less sensitive to such deviations. Zonal integration also avoids averaging local deposition rates over cell faces, which receive no accretion; thus it is local cell size independent. Deposition rates in units of kg/s were predicted for the zone upwind of the cooling-tower facility, on the cooling-tower complex, and on five ground and building zones. The remaining particles escaped out the end of the computational domain. Figs. 1 and 2 display the ground and building zones for a wind orientation of 180° for the isolated cooling-tower facility and the fully configured building cases, respectively.

4. Computational results and discussion

Zonal calculations were performed for four wind orientations (160°, 180°, 220°, and 240°), three wind speeds (2.5, 5.0, and 7.5 m/s measured at a height of 52 m with a velocity profile power law coefficient equal to 0.25), and droplets were emitted vertically in a air/vapor plume at 8.5 m/s from the cooling-tower units 1 through 11 at a rate of 1 kg/s and a Rosin–Rammler droplet distribution (characterized by a mean diameter of 0.1 mm, a minimum diameter of 0.01 mm, a maximum diameter of 1 mm, and a shape factor, n, equal to 1.0). Mass deposition rates (kg/s) were calculated for each zone for the four wind orientations, 160°, 180°, 220°, and 240°, respectively. Typical results for a reference wind speed, $U = 5$ m/s are shown in Table 1 for isolated cooling tower and cooling tower surrounded by a full set of buildings for four wind orientations. The difference between the values recorded for Total Trapped and Trapped Ground reflects deposition directly on the sides and roofs of buildings. Given the random number methodology used in the stochastic discrete particle method to generate particle paths, it was found that individual replications of deposition may vary $\pm 30\%$ around the average, but deposition trends are consistent.

4.1. Multiplication factors

The ratio of the mass accumulation rate for a given zone and a fully configured building case to the mass accumulation for the equivalent zone and the isolated cooling-tower facility case is designated here as a deposition multiplication factor (MF). Table 2 displays the MF values for the four wind orientations, 160°, 180°, 220°, and 240°, respectively. Figs. 15–17 display similar information in the form of bar charts.

Table 2 may be created from Table 1 by considering the ratio of magnitudes of deposition predicted over each zone taken without and with surrounding structures present. Note that MF appears to be largest for the 160° and 240° orientations.

- For the 160° orientation the cooling-tower cells are aligned along the windward axis so that all tower efflux would be expected to fall in a narrow band downwind of the cooling-tower complex; however, in the absence of upwind structures the vertical exhaust from downwind unit cells tend to deflect upwind cell plumes upward and delay drift descent. In the presence of up and downwind structures the individual plume trajectories are more thoroughly mixed, and turbulence generated by downwind

Table 1
Zonal deposition rates, $U = 5$ m/s, distances measured downwind of CT and boiler downwind edge

Arrangement	Isolated CT	Isolated CT	Isolated CT	Isolated CT	Structures present	Structures present	Structures present	Structures present
Wind angle	160°	180°	220°	240°	160°	180°	220°	240°
Distance, m (ft)	Mass rate (kg/s)	Mass rate (kg/s)	Mass rate (kg/s)	Mass rate (kg/s)	Mass rate (kg/s)	Mass rate (kg/s)	Mass rate (kg/s)	Mass rate (kg/s)
−305 to 0 (−1000 to 0)	0.0000	0.0102	0.0591	0.0000	0.0960	0.0740	0.1150	0.0780
0–76 (0–250)	0.0138	0.0491	0.0987	0.0815	0.1250	0.0955	0.0780	0.1290
76–152 (250–500)	0.0224	0.0381	0.0382	0.0371	0.1090	0.0666	0.0750	0.1180
152–229 (500–750)	0.0283	0.0306	0.0260	0.0143	0.0685	0.0336	0.0430	0.0400
229–305 (750–1000)	0.0152	0.0294	0.0136	0.0187	0.0220	0.0357	0.0090	0.0330
305–381 (1000–1250)	–	0.0155	0.0119	0.0197	0.0220	0.0194	0.0150	0.0100
CT and boiler roofs	0.0171	0.0632	0.0873	0.1260	0.1260	0.1850	0.1460	0.1130
Downwind outlet	0.9030	0.7639	0.6652	0.7100	0.4260	0.4820	0.5160	0.4710
Total trapped	0.0968	0.2361	0.3348	0.2973	0.5685	0.5098	0.4810	0.5210
Trapped ground	0.0797	0.1627	0.2884	0.1713	0.3465	0.2508	0.2200	0.3300
Mass balance	0.9998	1.0000	1.0000	1.0073	0.9945	0.9918	0.9970	0.9920

Table 2
Multiplication factors (MF), $U = 5$ m/s

Distance, m (ft)	MF 160°	MF 180°	MF 220°	MF 240°
0–76 (0–250)	9.06	1.951	0.79	1.58
76–152 (250–500)	4.87	1.75	1.96	3.18
152–229 (500–750)	2.42	1.10	1.65	2.80
229–305 (750–1000)	1.45	1.21	0.66	1.76
305–381 (1000–1250)	–	1.25	1.26	0.51
Average	4.45	1.45	1.27	1.97
Total trapped	5.87	2.16	1.44	1.75
Trapped ground	4.35	1.54	1.17	1.93

structures enhances vertical motion increasing the likelihood that droplets will reach the ground near the tower. As wind speed increases MF decreases, but the maximum values remain near the source (see Fig. 15).

- For the 240° orientation the wind is directed perpendicular to the row of individual cooling-tower cells which limits plume interaction and tends to spread the drift over a wide lateral region; however, the two very tall (175 m) structures are now so positioned that they produce a jet between the buildings that deflects the plumes almost to the ground. This carries heavy particles further downwind before they reach ground, which

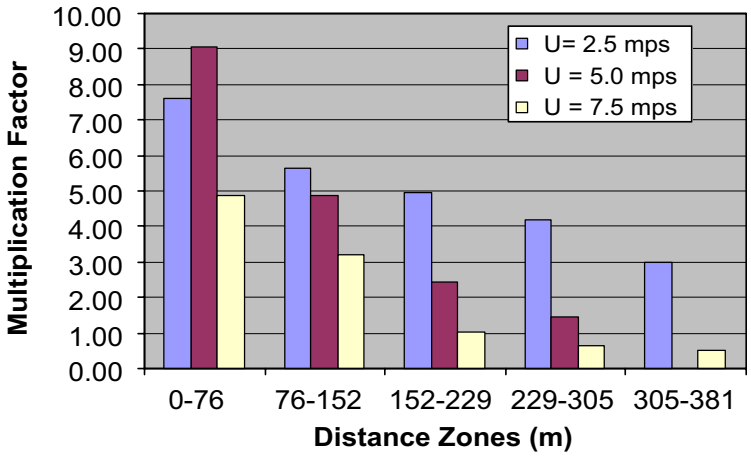

Fig. 15. Zonal MF 160°, $U = 2.5$–7.5 mps.

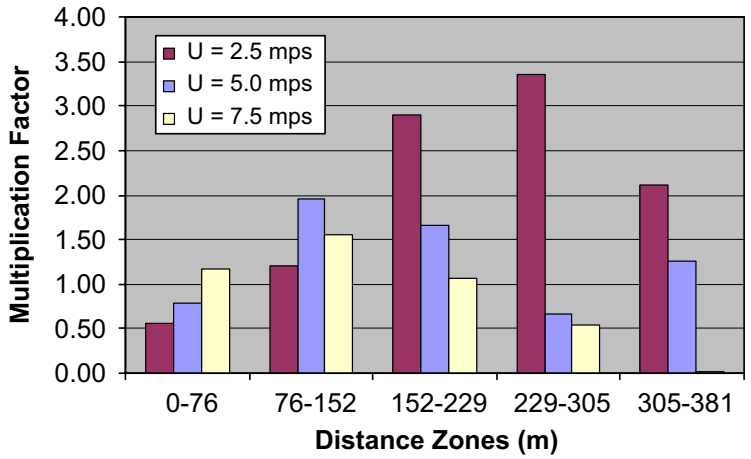

Fig. 16. Zonal MF 240°, $U = 2.5$–7.5 mps.

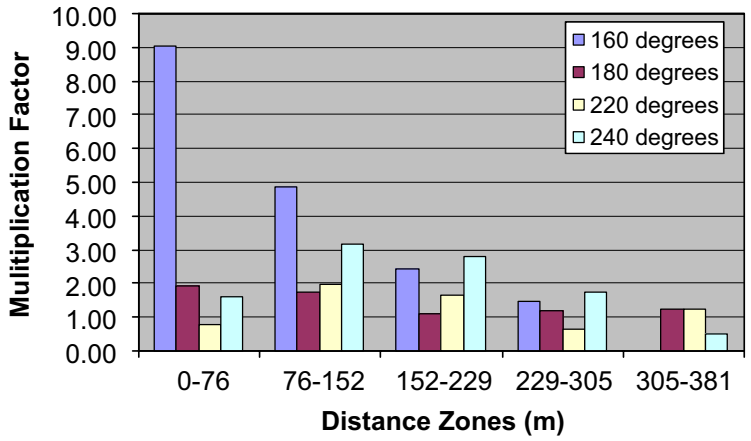

Fig. 17. Zonal MF 160–240°, $U = 5$ mps.

produces MF < 1 for distances < 76 m but increases deposition at greater distances. As wind speed increases the MF decreases, but the maximum value also occurs closer to the source (see Fig. 16).

Note that MF magnitudes tend to be maximum at or near the source, and subsequently decrease downwind, Fig. 17. Given that the ground acts as a mass sink, mass continuity requires that at greater distances the MF approaches one, then values less than one, and, finally, asymptotes to one again. This effect is also evident in Table 1 where one notes that more drift mass is trapped within the computational domain for cases with surrounding building structures present.

4.2. Average MF

If one averages the five zonal deposition MF one obtains the average multiplication factor (AMF) for a given wind orientation. Thus, the final product of the additional calculations might be a set of four AMF values to be interpolated among wind sectors used during ISC or SACTI annual calculations. One might ask "why calculate AMF when MF contain the same information in greater detail?" Discussion with consultants who routinely ran codes like ISC and SACTI revealed that it would be difficult to integrate more specific near-field distance variations into these codes; hence, the average values were proposed for cases where deposition effects were expected to be limited to short downwind distances (<0.5 km).

Table 3 and Fig. 18 display the predicted influence of approach wind speed on zonal deposition through the AMF. As the approach wind increases the cooling-tower plumes are deflected closer to the ground even in the absence of surrounding building effects. Thus the anticipated effect of surrounding structures is reduced since the droplets are already

Table 3
Average multiplication factors (AMF)

Velocities	AMF 160°	AMF 180°	AMF 220°	AMF 240°
$U = 2.5$ mps	5.60	–	–	2.03
$U = 5.0$ mps	4.45	1.45	1.27	1.97
$U = 7.5$ mps	4.40	–	–	1.09
Average	4.82	1.45	1.27	1.69

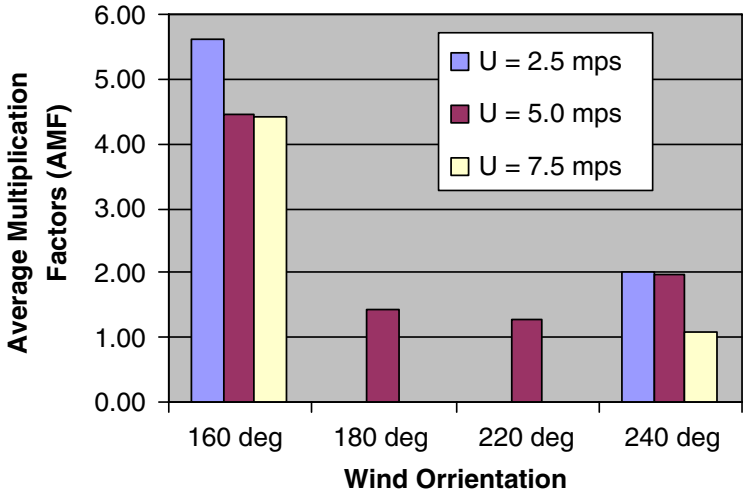

Fig. 18. Zonal AMF, 160–240°, $U = 2.5$–7.5 mps.

closer to the ground surface. Conceivably, given an efficacious height and position of upwind buildings, deposition values might be reduced with increased wind speed due to the sheltering of cooling-tower plumes in the building wakes. In these situations MF or AMF may sometimes be less than 1.0 in the near-field distances.

5. Conclusions

A protocol is proposed to generate a typical set of coefficients that might be used to adjust the results of seasonal or annual deposition predictions using analytic programs such as ISC Prime or SATCI. The multiplicative and average multiplicative factors (MF and AMF) produced are based on reasonable scientific certainty concerning the physics of the fluid processes and the analytic and computational methods employed.

References

Bahmann, W., Schmonsees, N., 2004. Consideration of wind tunnel studies in dispersion calculations with the New Model AUSTAL2000—case study: discharge of flue gas via cooling towers. In: Proceedings of 9th International Conference on Harmonisation with Atmosperic Dispersion Modelling for Regulatory Purposes, Garmisch-Partenkirchen, Germany, 1–4 June 2004, pp. 188–191 〈http://www.harmo.org/conferences/proceedings/_garmisch/publishedSections/2.01.pdf〉.

Bender, T.J., et al., 1996a. A study on the effects of wind on the air intake flow rate of a cooling tower: part 2. Wind wall study. J. Wind Eng. Ind. Aerodyn. 64, 61–72.

Bender, T.J., et al., 1996b. A study on the effects of wind on the air intake flow rate of a cooling tower: part 3. Numerical study. J. Wind Eng. Ind. Aerodyn. 64, 73–88.

Bergstrom, D.J., et al., 1993. Numerical study of wind flow over a cooling tower. J. Wind Eng. Ind. Aerodyn. 46 & 47, 657–664.

Blocken, B., Carmeliet, J., 2006. The influence of the wind-blocking effect by a building on its wind-driven rain exposure. J. Wind Eng. Ind. Aerodyn. 94, 101–127.

Blocken, B., et al., 2006. Impact of wind on the spatial distribution of rain over micro-scale topograph: numerical modeling and experimental verification. Hydrol. Process 20, 345–368.

Brucher, W., 2001. Simulation of terrain amplification factors for annual concentration statistics using a Lagrangian particle dispersion model. In: Proceedings of 7th International Conference on Harmonisation within Atmospheric Dispersion Modelling for Regulatory Purposes, Session 3: Short Distance Dispersion Modelling, Belgirate, Italy, 28–31 May 2001, pp. 207–211 〈http://www.aqm.jrc.it/harmo7/p207.pdf〉.

Derksen, D.D., et al., 1996. A study on the effects of wind on the air intake flow rate of a cooling tower: part 1. Wind tunnel study. J. Wind Eng. Ind. Aerodyn. 64, 47–59.

England, W.G., et al., 1973. Cooling tower plumes-defined and traced by means of computer simulation models. 1973 Cooling Tower Institute Annual Meeting, Houston TX-January 29–31, p. 41.

Fluent 6.1 User's Guide, 2003. Available on web by permission from Fluent at: 〈http://www.fluentusers.com/fluent61/doc/doc_f.htm〉.

Lawson Jr., R.E., et al., 1989. Estimation of maximum surface concentrations from sources near complex terrain in neutral flow. Atmos. Environ. 23 (2), 321–331.

Meroney, R.N., 2006. CFD prediction of cooling tower drift. J. Wind Eng. Ind. Aerodyn. 94 (6), 463–490.

Policastro, A.J., et al., 1981. Studies on Mathematical Models for Characterizing Plume and drift Behavior from Cooling Towers, Vol. 3: Mathematical Model for Single-Source (Single-Tower) Cooling Tower Drift Dispersion, CS-1683, Vol. 3, Research Project 906-2, Argonne National Laboratory, Prepared for Electric Power Research Institute, Palo Alto, CA.

Snyder, W.H., 1990. Fluid modeling to atmosperhic diffusion in complex terrain. Atmos. Environ. 24A, 2071–2088.

Takata, K., et al., 1996. Prediction of the plume from a cooling tower. In: 1996 Cooling Tower Institute Annual Conference, Houston, TX-February 1996, p. 27.

U.S. EPA, 1995. User's Guide for the Industrial Source Complex (ISC3) Dispersion Models: Volume II—Description of Model Algorithms, EPA-454/B-95-003b, pp. 1:5–1:30 and 1:35–1:46.

Yoshie, R., et al., 2006. CFD prediction of wind environment around a high-rise building located in an urban area. In: Proceedings of 4th International Symposium On Computational Wind Engineering, Yokohama, Japan 16–19 July 2006, pp. 129–132.

Zhang, A., et al., 2005. Numerical simulation of the wind field around different building arrangements. J. Wind Eng. Ind. Aerodyn. 93, 891–904.